Date of publication xxxx 00, 0000, date of current version xxxx 00, 0000.

Digital Object Identifier 10.1109/ACCESS.2017.DOI

Efficiency of NOMA-Assisted FD-AF vehicle-to-vehicle Relaying over Nakagami-m Fading Channels

SAJID HUSSAIN ALVI[1], MOHAMMAD ARIF[2,*], and KEIVAN NAVAIE[3,*]
[1]Department of Physics, COMSATS University Islamabad, Islamabad 45550, Pakistan.
[2]Department of Computer Engineering, Gachon University, Seongnam-si 13120, South Korea.
[3]School of Computing and Communications, Lancaster University, LA1 4WA Lancaster, U.K.

*Corresponding author: Mohammad Arif (e-mail: mohammadarif911@gachon.ac.kr) and Keivan Navaie (e-mail: k.navaie@lancaster.ac.uk).

"This work was partly funded by Lancaster University, UK."

ABSTRACT Nakagami-m distribution is typically used to model various multipath fading channels in relaying networks. This work analyses a NOMA-based vehicle-to-vehicle (V2V) relaying over Nakagami-m fading channels. Specifically, we investigate the performance of a NOMA over the Nakagami-m distributed channels by leveraging a dual-hop full-duplex amplify-and-forward scheme in V2V communications. To this end, we derive closed-form expressions of rate outage probabilities and average received signal-to-interference plus noise ratios for the two vehicular users at non-identical destinations in terms of Tricomi confluent hypergeometric function. The derived analytical results are valid for arbitrary values of the fading parameter m. Furthermore, we also derive the expressions for the lower and upper bounds on rate outage probabilities. The residual self-interference, inherent in the full-duplex V2V relaying is also considered and its impact on the system's performance is studied. The accuracy of the analytical expressions is validated by simulation results which are found to be in good agreement.

INDEX TERMS V2V communication, Amplify-and-forward relaying, Fox's H-function, Full-Duplex, NOMA, Outage analysis

I. INTRODUCTION

HIGH data rate throughput, low latency, efficient utilization of resources, e.g., energy and spectrum are the key demands of beyond fifth-generation wireless networks [1]. In recent years, the non-orthogonal multiple access (NOMA) approach has been recognized as a viable option for improving frequency and energy usage of wireless networks. Conventionally, the power-based NOMA scheme uses the multiplexing of signals by considering their power-domain to overlay numerous subscriber transmissions on a channel. The resulting signal is sent via exploiting frequency as well as time resources. Following which, the successive interference cancellation (SIC) approach is used at the other end of the receiver to extract the overlaid information. NOMA outperforms conventional multiple access with regard to the delay, transmission rate, and frequency [2].

Vehicular communication is becoming essential because of its potential uses in self-driving smart cars. Smart cars provide vehicle-to-vehicle (V2V) connections and vehicle-to-infrastructure (V2I) connections, allowing users to exploit high-capacity network services without compromising their speeds on the highways. Vehicular communication employs two distinct units such as the on-board unit (OBU) and the road-side unit (RSU) [3]–[7]. OBU is placed on a vehicle-node and conventionally consists of sensing device, controller unit device, and multiple antennas (for transmission and reception of signals). The main purpose of the on-board equipment is to receive transmission or relay transmission. RSU is typically a non-movable device and is located near highways for the purpose of direct communication between vehicle node and infrastructure or another adjacent RSU. Vehicular transmissions face severe fading effects than the traditional wireless channels. This is because of the parameters involving increased mobility, variable surroundings, limited antenna heights, and quick signal fluctuations for vehicular transmissions. Such circumstances result in complicated multipath transmission, large doppler shifts, and time-selective fading, making receiving signals more diffi-

cult than in classic wireless channels [8]. As a result, the transmission between V2V and V2I devices will have poor overall network efficiency than typical wireless networks. Consequently, characterizing the performance of a typical vehicle node in a severe fading environment is crucial to investigate the efficiency of the vehicular communications [9].

Half-duplex relaying distributes the data transfer and reception over discrete time slots, reducing spectral effectiveness while preventing self-interference. Full-duplex relaying enables simultaneous data transfer and reception, possibly increasing spectrum efficacy by incorporating interference signals that require sophisticated cancelation approaches. However, although full-duplex relaying provides faster capacity, it increases complexity in systems and hardware requirements. The decision to select half and full duplexing is determined by considerations such as controlling interfering signals, spectrum effectiveness, and architecture limitations [10]. Half-duplex and full-duplex models exploiting NOMA techniques have been considered for investigating the performance of vehicular communications and it has been shown that full-duplex vehicular networks have improved performance than the traditional half-duplex networks [11]–[13]. Transmission and reception of signals over the same frequency channel can double the spectral efficiency [14], [15] as well as extend the communication range using full-duplex relaying, albeit inevitable residual self-interference (RSI). NOMA allows multiple users to transmit their signals through sharing the time and frequency resources by employing power domain multiplexing. This not only enhances the spectral efficiency but also provides massive connectivity [16].

Decode-and-forward technique analyzes the obtained message, re-encodes it, and afterward transmits it, thereby removing noise while incurring more time and computational capacity [17]. While amplify-and-forward technique merely intensifies the message that it received, containing all background noise, prior to sending it back again, which makes it a less complicated and low-latency method but prone to noise transmissions [18]. Decode-and-forward is desirable in situations when reliability of signals is vital, but amplify-and-forward is beneficial for applications requiring less power and complexity. The decision amid these approaches is contingent upon the network limitations including power, delay, or controlling interference. Amplify-and-Forward (AF) relaying is considered useful in V2V communications due its simplicity and ease of deployment. Hence, NOMA combined with full-duplex amplify-and-forward (FD-AF) relaying in V2V communications comes up with performance gains that increases the gravity of these protocols remarkably.

A. RELATED WORK

NOMA-based full-duplex relaying have been investigated in [1], [14]–[16], [19], whereas NOMA-based relaying in V2V communications is discussed in [20], [21]. A full-duplex relay aided NOMA system using partial relay selection is addressed in [1]. Exact analytical expressions of outage probability (OP) and ergodic capacity (EC) are derived. The impact of number of relays, power allocation parameter and RSI on these performance metrics is studied. An energy-harvesting enabled full-duplex relay system is analyzed in [14]. Closed-form expressions of OP and ergodic rates are obtained for the scenario where the energy deficient full-duplex relay harvests energy from the source node. Their analysis reveal that this system has performance gains over the conventional NOMA supported full-duplex relay system. An edge catching enabled full-duplex NOMA system is investigated in [15]. Optimization of successful offloading probability through scalable power allocation is performed. NOMA is benefited for direct and relay transmission to facilitate the edge node as well as to efficiently utilize the bandwidth. Transmission, detection and power allocation based uplink with NOMA and cooperative-rate splitting-multiple-access (C-RSMA) based system is examined in [16]. The achievable rates of cooperative-NOMA and C-RSMA schemes are studied. Moreover, asymptotic OP expressions showing the diversity order of two are also derived for the both schemes. Switching-assisted cognitive NOMA with transmit antenna and user selection scheme is probed in [19]. A cooperative NOMA that is underlay to a primary network such that a selected near secondary user cooperates to a far secondary user using the full-duplex mode by appointing the interference temperature limit. Optimization techniques are used to maximize the minimum rates of two users considering proportional fairness coefficient. Analytical expressions of OP are derived for both users assuming imperfect SIC at the near user.

Performance analysis of uplink NOMA coordinated FD-AF relaying is carried out in [22]. An approximate OP expression is derived and the impact of power allocation and various threshold values on OP are analyzed. It is worth mentioning that all the works cited above considered Rayleigh fading at all the links for analysis of their systems. However, few works are available in the literature on the performance analysis of full-duplex relaying with NOMA over Nakagami-m fading channels [23], [24]. A virtual full-duplex (VFD) decode-and-forward (DF) relaying with NOMA considering imperfect SIC and RSI is investigated in [23]. OP, asymptotic OP and ergodic rate expressions are developed for the considered system. A VFD NOMA system in which source transmits two messages to two different users as well as to a destination node in three different time slots is addressed in [24]. A novel transmission strategy under imperfect SIC and RSI is proposed and the results showed that the OP reduces at the destination node.

Literature is enriched with the analysis of NOMA aided half-duplex relaying over Nakagami-m fading channels [25], [26], [28]. Half-duplex amplify-and-forward (HD-AF) relaying system is taken up by [25] in which closed-form expressions of the moments and rate outage of the received instantaneous signal-to-interference plus noise ratios (SINRs) are acquired. The authors disclosed that system performs

TABLE 1: Recent researches, their considered models, contributions and limitations.

Ref.	System Model	Outcomes	Limitations
[1]	FD-relay aided NOMA	Outage probability and ergodic capacity derivations	Analysis of FD-AF relaying with NOMA
[14]	Energy harvesting FD-relay aided NOMA	Outage probability and ergodic capacity derivations	Analysis of FD-AF relaying with NOMA
[16]	C-RSMA disrupting NOMA	Ergodic rate analysis	Outage probability not analyzed
[23]	VFD considering DF relaying with NOMA	Outage probability and ergodic rate analysis	Analysis of FD-AF relaying with NOMA
[25]	Analysis of HD-AF with Nakagami-m	Closed-form expressions of rate outage	Analysis of FD-AF relaying with NOMA
[26]	Analysis of Fixed gain AF relaying with NOMA	Analysis of rate outage probability	Analysis of FD-AF relaying with NOMA
[27]	IRS-aided NOMA considering HD-DF	Upper and lower bounds on power allocation coefficients	Analysis of FD-AF relaying with NOMA
This work	Analysis of FD-AF relaying with NOMA with Nakagami-m fading	Rate outage probability analysis; lower and upper bounds on rate outage probability analysis	–

best when the relay is located at the center between source and destination nodes. Downlink NOMA system with partial channel state information (CSI) is considered in [28]. Closed-form expressions of OP and ergodic sum rate for DF relaying whereas asymptotic expressions for AF relaying are derived. Their analysis declares the performance superiority of DF over AF in terms of both performance parameters.

Fixed-gain AF continues to be employed more recently, albeit dynamic gain AF's superior efficiency, since its implementation is less complicated, does not need real-time channel estimate, and reduces equipment complexity. Variable gain AF demands computing delays, hence fixed gain AF is suited for power-constrained and real-time tasks whereby flexibility might not be important. Analysis of a fixed-gain AF relaying system with NOMA considering two scenarios is presented in [26]. Base station communicates to multiple users with the help of AF relaying taking into account the direct link in first scenario whereas AF relay is absent in the second scenario. Closed-form exact and asymptotic expressions of OP are derived for both scenarios unveiling the supremacy of NOMA over OMA. NOMA systems with and without relaying are investigated over other fading channels as well, e.g., see [27], [29]. A comparison of intelligent reflecting surface (IRS) aided NOMA with half-duplex DF relay assisted NOMA is presented in [27]. A power allocation scheme is developed based on the number of IRS elements. Moreover, lower and upper bounds on the power allocation coefficients are also proposed. Their analysis reveal the superiority of IRS-assisted NOMA over relay-coordinated NOMA. A transceiver design using minimum shift keying (MSK) for an asynchronous uplink NOMA is provided in [29]. Complexity analysis of the various detection schemes is proposed. However, [27], [29] have not considered Nakagami-m fading channels for NOMA schemes that can consider multiple severities in V2V communications. A list of recent works, their network models, contributions, and limitations are discussed in Tab. 1.

B. MOTIVATION AND CONTRIBUTION

Nakagami-m distribution is well-known for modeling various multipath fading scenarios with fading parameter, m. The flexibility of the fading parameter, m makes Nakagami-m distribution a good candidate for a fading channel model. It models worst than Rayleigh fading ($0.5 \leq m < 1$), Rayleigh fading ($m = 1$) and less severe than Rayleigh fading ($m > 1$) [30], [31]. When $m \to \infty$, it converges to a non-fading channel named additive white Gaussian noise (AWGN) channel [31]. In all the aforementioned researches, fading severities by considering Nakagami-m for a NOMA-coordinated FD-AF V2V network is not analyzed which can model multiple fading scenarios. Motivated by this research gap, in this paper, the authors examine the performance of a NOMA-coordinated FD-AF relaying V2V network considering different fading severities at all the links by making use of Nakagami-m distribution. The major contributions of the presented work can be summarized as follows:

- Novel closed-form expressions of rate outage probabilities for two users located at dissimilar locations are derived, valid for arbitrary values of the fading parameter m.
- The upper and lower bound expressions on rate outage probabilities are deduced from the derived expressions.
- Closed-form expressions of average received SINRs are derived for the same system, valid for any value of the fading parameter m.
- The impact of RSI due to full-duplex relaying on the performance of the system is studied.

The performance metrics addressed in the presented work have practical significance, e.g., OP is considered useful performance measure for ergodic systems. When the transmitters do not have knowledge of CSI, OP is considered more meaningful performance parameter in delay sensitive

TABLE 2: Notations and their descriptions.

Parameter	Description
S, R, D_1, D_2	Source, relay, destination vehicle 1, and destination vehicle 2
s_1, s_2	Transmitted symbols 1 and 2
a_1, a_2	NOMA powers for s_1 and s_2, resp.
P_S, P_R	Transmit power of source and relay
g_{ij}	Fading channel coefficients between the nodes i and j
D_{ij}	Distance-dependent pathloss between the nodes i and j
ν	Pathloss exponent
n_R	Zero mean thermal Gaussian noise added at the relay node
n_{Dj}	Zero mean thermal Gaussian noise added at the j-th destination
σ_j^2	Average power of AWGN added at the j-th node
m_{ij}	Fading severity parameter for the link between i-th and j-th node
γ_{ij}	Instantaneous SNR for the link between i-th and j-th node
x_R	Signal transmitted by the relay
y_R	Signal received by the relay
T_{PD}	Processing delay at the relay node
Ω_{SR}	Average power gains of S-R fading channel
Ω_{RR}	Average power gains of RSI fading channels
λ_{RR}	Average RSI power
β	Gain of the received signal
r_1, r_2	Threshold for rate outage of D_1 and D_2

scenarios to implement the quality of service. Similarly, the average signal-to-noise ratio (SNR) is used in a multi relay system to select the best relay as well in various optimization algorithms to attain an optimal threshold [32].

C. ORGANIZATION

The remainder of this paper is organized as follows. The system and channel model are explained in Section II and details of the performance analysis are provided in Section III. Some numerical results of the proposed analysis are discussed in Section IV, whereas concluding remarks are given in Section V.

The notations used in this paper are given in Tab. 2.

II. SYSTEM AND CHANNEL MODEL

Consider a dual-hop relayed V2V network consisting of a source, a fixed-gain FD-AF relay and two destination vehicle nodes as shown in Fig. 1. These nodes are represented by S, R, D_1 and D_2, respectively. The direct link is assumed to be unavailable owning to severe channel degradation in the considered scenario. The S, D_1 and D_2 are assembled with single antennas while relay is arrayed with two antennas, one for transmission and other for reception of signals. Full-duplex relaying suffers from RSI which degrades the system's performance. The source with power P_S transmits two symbols $s_1(t)$ and $s_2(t)$ using the superposition coding $x_S(t) = \sqrt{P_s a_1}\, s_1(t) + \sqrt{P_s a_2}\, s_2(t)$ with the help of FD-AF relay to the two NOMA vehicular users present at D_1 and D_2, respectively. Moreover, a_1 and a_2 are NOMA power levels such that $a_1 + a_2 = 1$ and $a_1 > a_2$. This power distribution ensures more power allocation to weak vehicular user, i.e., D_1 and less power to strong vehicular user, i.e., D_2 as per NOMA scheme. The proposed setup assumes that $R-D_2$ link has better fading channel conditions than $R-D_1$ link [1]. Let h_{ij}=$g_{ij}D_{ij}^{-\frac{\nu}{2}}$, where $i, j \in (S, R, D_1, D_2)$ denote the flat fading channel coefficients between the nodes i and j capturing the effect of multipath fading, i.e., g_{ij} and distance-dependent pathloss, i.e., $D_{ij}^{-\frac{\nu}{2}}$ whereof ν signifies as the pathloss exponent [33]. Then the signal received at the relay can be written as [1]

$$y_R(t) = h_{SR}\, x_S(t) + h_{RR}\, x_R(t) + n_R(t), \tag{1}$$

where h_{RR} is the Rayleigh distributed RSI [1], [34] whereas $n_R(t)$ represents the zero mean thermal Gaussian noise added at the relay node. The signal transmitted by the relay after amplification can be written as

$$x_R(t) = \beta\, y_R(t - T_{PD}), \tag{2}$$

wherein $E\{|x_R(t)|^2\}$=$\beta^2 E\{|y_R(t-T_{PD})|^2\}$=$P_R$ [35]. It may be noted that P_R is the transmit power of the relay whereas T_{PD} is the processing delay at the relay node. When CSI of the source-relay (S-R) link is unknown at the relay node, then it amplifies the received signal with a fixed gain β [34] as

$$\beta = \sqrt{\frac{P_R}{P_S\,\Omega_{SR} + P_R\Omega_{RR} + \sigma_R^2}}, \tag{3}$$

where Ω_{SR}=$E\{|h_{SR}|^2\}$=$E\{|g_{SR}|^2\}\, D_{SR}^{-\nu}$ and $\Omega_{RR} = E\{|h_{RR}|^2\}$ represent the average power gains of S-R and RSI fading channels, respectively. Furthermore, we define λ_{RR}=$P_R\Omega_{RR}$ as the average RSI power. The signal received by the first vehicular user at D_1 can be written as

$$\begin{aligned} y_{D1}(t) &= \beta\, h_{RD1}\, y_R(t - T_{PD}) + n_{D1}(t) \\ &= \beta\, h_{SR}\, h_{RD1} \sqrt{P_s a_1}\, s_1(t - T_{PD}) \\ &+ \beta\, h_{SR}\, h_{RD1} \sqrt{P_s a_2}\, s_2(t - T_{PD}) \\ &+ \beta\, h_{RD1}\, h_{RR}\, x_R(t - T_{PD}) \\ &+ \beta\, h_{RD1}\, n_R(t - T_{PD}) + n_{D1}(t), \end{aligned} \tag{4}$$

where $n_{D1}(t)$ characterize the zero mean thermal Gaussian noise added at the first vehicle destination. Now taking square of $|y_{D1}(t)|$ and operating the expectation over $|h_{RR}|^2$, $|n_R(t)|^2$ and $|n_{D1}(t)|^2$, we have

$$\begin{aligned} E\{|y_{D1}(t)|^2\} &= |\beta|^2\, |h_{SR}|^2\, |h_{RD1}|^2\, P_s\, a_1 \\ &+ |\beta|^2\, |h_{SR}|^2\, |h_{RD1}|^2\, P_s\, a_2 \\ &+ |\beta|^2\, |h_{RD1}|^2\, \Omega_{RR} P_R \\ &+ |\beta|^2\, |h_{RD1}|^2\, \sigma_R^2 + \sigma_{D1}^2, \end{aligned} \tag{5}$$

where we considered $E\{|s_1|\}$=$E\{|s_2|\}$=$E\{|n_R|\}$=$E\{|n_{D1}|\}$=0, $E\{|s_1|^2\}$=$E\{|s_2|^2\}$=1, $E\{|n_R|^2\}$=σ_R^2 and $E\{|n_{D1}|^2\}$=σ_{D1}^2. Similar mathematical procedure is followed in writing $|y_{D12}(t)|^2$ and $|y_{D2}(t)|^2$ and then operating the expectation over $|h_{RR}|^2$, $|n_R(t)|^2$ and $|n_{D2}(t)|^2$.

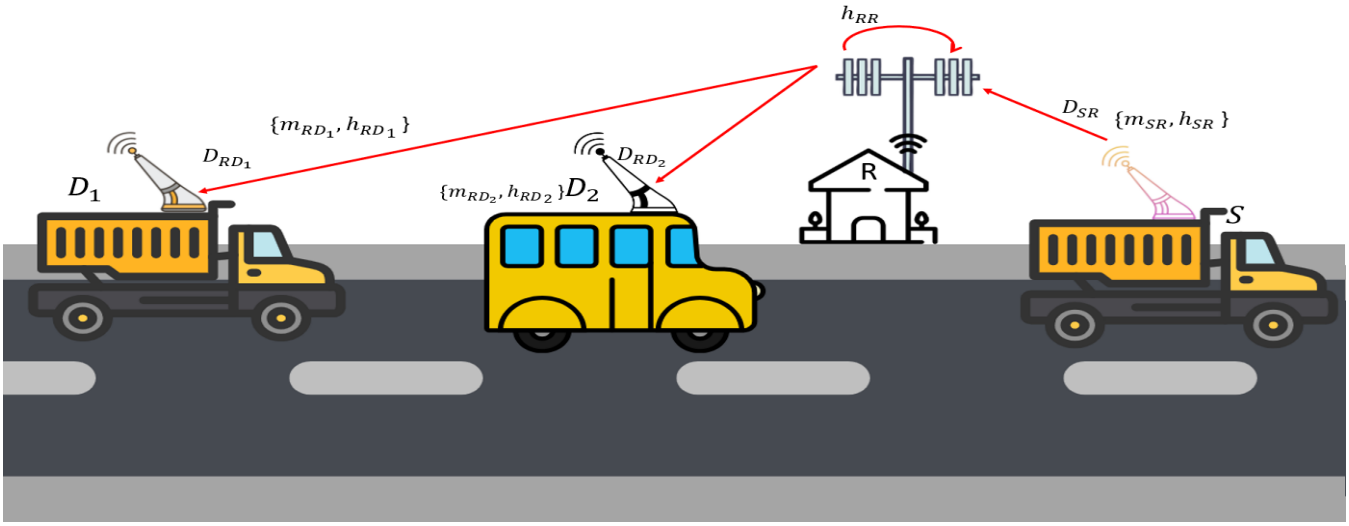

FIGURE 1: System model under consideration.

Let $\gamma_{ij} = \frac{P_i}{\sigma_j^2}|h_{ij}|^2$ typify the gamma distributed instantaneous SNR of the corresponding link in which σ_j^2 represents the average power of AWGN added at the respective nodes. Then it's probability density function (PDF) can be written as [36, Eq. (2.28b)]

$$f_{\gamma_{ij}}(\gamma_{ij}) = \frac{m_{ij}^{m_{ij}} \gamma_{ij}^{m_{ij}-1}}{\lambda_{ij}^{m_{ij}} \Gamma(m_{ij})} exp\left(-\frac{m_{ij}\gamma_{ij}}{\lambda_{ij}}\right), \quad \gamma_{ij} \geq 0 \qquad (6)$$

where m_{ij} is the fading severity parameter for the respective link and $\Gamma(\cdot)$ is the gamma function [37, Eq. (8.310.1))]. It is mandatory to mention that λ_{ij}=$\frac{P_i}{\sigma_j^2}E\{|h_{ij}|^2\}$ = $\frac{P_i}{\sigma_j^2}E\left\{|g_{ij}|^2\right\}D_{ij}^{-v}$ stands for the average received SNR of the considered link. The PDF expression can also be manifested in terms of Fox's H-function using [38, Eq. (1.7.2)] and [38, Eq. (1.2.4)] as

$$f_{\gamma_{ij}}(\gamma_{ij}) = \frac{\left(\frac{m_{ij}}{\lambda_{ij}}\right)}{\Gamma(m_{ij})} H_{0,1}^{1,0}\left[\frac{m_{ij}\gamma_{ij}}{\lambda_{ij}}\middle|(m_{ij}-1,1)\right], \qquad (7)$$

where $H_{p,q}^{m,n}[\cdot]$ is the Fox's H-function [38, Eq. (1.1.1)]. The cumulative distribution function (CDF) of γ_{ij} can be written as [36, Eq. (2.29b)]

$$F_{\gamma_{ij}}(\gamma_{ij}) = 1 - \frac{1}{\Gamma(m_{ij})}\Gamma\left(m_{ij}, \frac{m_{ij}\gamma_{ij}}{\lambda_{ij}}\right), \ \gamma_{ij} \geq 0, \qquad (8)$$

where $\Gamma(\cdot,\cdot)$ is the upper incomplete gamma function [37, Eq. (8.350.2)].

III. PERFORMANCE ANALYSIS

The performance of the NOMA-enabled FD-AF relay network is analyzed by considering end-to-end SINR equations. The equation (4) facilitate us to write end-to-end SINR expressions at D_1 and D_2, respectively. The received instantaneous SINR at D_1 can be written using (5) as

$$\gamma_{D1} = \frac{a_1\,\gamma_{SR}\,\gamma_{RD1}}{a_2\,\gamma_{SR}\,\gamma_{RD1} + C_2\,\gamma_{RD1} + C_1}, \qquad (9)$$

where C_2=$\frac{\lambda_{RR}}{\sigma_R^2} + 1$ and C_1=λ_{SR}+C_2. The strong user at D_2 plays significant role in a sense that it first decodes the signal intended for the weak user at D_1 and then remove it using SIC. After that it decodes its own signal according to NOMA scheme [1]. Therefore, the received instantaneous SINR at D_2 relative to D_1 can be drafted as

$$\gamma_{D12} = \frac{a_1\,\gamma_{SR}\,\gamma_{RD2}}{a_2\,\gamma_{SR}\,\gamma_{RD2} + C_2\,\gamma_{RD2} + C_1}. \qquad (10)$$

After perfect SIC implementation at D_2, the received instantaneous SINR at D_2 can then be penned as

$$\gamma_{D2} = \frac{a_2\,\gamma_{SR}\,\gamma_{RD2}}{C_2\,\gamma_{RD2} + C_1}. \qquad (11)$$

Now we propose five theorems to analyze the proposed system. For this purpose, we define three Gamma distributed random variables denoted by X, Y_1 and Y_2 which represent the link SNRs, γ_{SR}, γ_{RD1} and γ_{RD2}, respectively. Their average values λ_x, λ_{y1} and λ_{y2} corresponds to average SNRs λ_{SR}, λ_{RD1} and λ_{RD2}, respectively. Similarly, the received instantaneous SINRs γ_{D1}, γ_{D12} and γ_{D2} are denoted by Z_1, Z_2 and Z_3. The average received SINRs $\overline{\gamma}_{D1}$, $\overline{\gamma}_{D12}$ and $\overline{\gamma}_{D2}$ are represented by $\overline{Z}_1$, $\overline{Z}_2$ and $\overline{Z}_3$, respectively. Moreover, we use $a = a_1$, $b = a_2$, m_1=m_{SR}, m_{21}=m_{RD1} and m_{22}=m_{RD2} for notational convenience.

A. RATE OUTAGE ANALYSIS

A rate outage is defined as the probability that the maximum attainable instantaneous throughput drops below the desired rate, r. It is given as $P_{out} = \Pr\{\log_2(1+\gamma) < r\}$. Consider $\mathbf{r} = 2^r - 1$ be the threshold then the outage probability is given as $P_{out} = \Pr\{\gamma < \mathbf{r}\}$. The rate outage probability of D1 is defined

as the probability that the received SINR of D1 falls below the threshold, r_1 and is derived in Theorem 1. The upper and lower bounds on the rate outage probability of D1 are derived as Corollary 1.1 and Corollary 1.2, respectively.

Theorem 1. *Let the random variables X, Y_1 and Y_2 be related to Z_1 through $Z_1 = \frac{aXY_1}{bXY_1+C_2Y_1+C_1}$, then the rate outage at D_1 can be written as*

$$P_{out1} = 1 - \frac{\left(\frac{m_1C_1}{\lambda_x} + \frac{m_1C_2\tilde{\theta}}{\lambda_x}\right)^{m_1}\left(\frac{m_{21}\tilde{\theta}}{\lambda_{y1}}\right)^{m_{21}}}{\Gamma(m_1)\Gamma(m_{21})} \times exp\left(-\frac{m_1C_1}{\lambda_x} - \frac{m_1C_2\tilde{\theta}}{\lambda_x}\right) exp\left(-\frac{m_{21}\tilde{\theta}}{\lambda_{y1}}\right) \times \sum_{n=0}^{\infty}\left(\frac{C_1}{C_1+C_2\tilde{\theta}}\right)^n \Psi\left(1+n, 1+m_{21}, \frac{m_{21}\tilde{\theta}}{\lambda_{y1}}\right) \times \Psi\left(1-n, 1+m_1-n, \frac{m_1C_1}{\lambda_x} + \frac{m_1C_2\tilde{\theta}}{\lambda_x}\right), \quad (12)$$

where $\Psi(\cdot,\cdot,\cdot,)$ is the Tricomi confluent hypergeometric function [37, Eq. (9.211.4)].
Proof: Please refer to Appendix A.

Corollary 1. *The Bernoulli inequality [39] facilitates us as*

$$\left(\frac{m_1C_1}{\lambda_x}\right)^{m_1}\left(1 + \frac{m_1C_2\tilde{\theta}}{C_1}\right) \leq \left(\frac{m_1C_1}{\lambda_x} + \frac{m_1C_2\tilde{\theta}}{\lambda_x}\right), m_1 \geq 1. \quad (13)$$

Substituting the lower bound of (13) in (12), we obtain an upper bound on P_{out1} as

$$P_{out1} \leq P_{out1}^{UB} = 1 - \frac{\left(\frac{m_1C_1}{\lambda_x}\right)^{m_1}\left(1 + \frac{m_1C_2\tilde{\theta}}{C_1}\right)\left(\frac{m_{21}\tilde{\theta}}{\lambda_{y1}}\right)^{m_{21}}}{\Gamma(m_1)\Gamma(m_{21})} \times exp\left(-\frac{m_1C_1}{\lambda_x} - \frac{m_1C_2\tilde{\theta}}{\lambda_x}\right) exp\left(-\frac{m_{21}\tilde{\theta}}{\lambda_{y1}}\right) \times \sum_{n=0}^{\infty}\left(\frac{C_1}{C_1+C_2\tilde{\theta}}\right)^n \Psi\left(1+n, 1+m_{21}, \frac{m_{21}\tilde{\theta}}{\lambda_{y1}}\right) \times \Psi\left(1-n, 1+m_1-n, \frac{m_1C_1}{\lambda_x} + \frac{m_1C_2\tilde{\theta}}{\lambda_x}\right), \quad (14)$$

Corollary 2. *The exponential function inequality [40, Eq. (4.2.30)] gives*

$$exp\left(-\frac{m_{21}\tilde{\theta}}{\lambda_{y1}}\right) < \frac{1}{\left(1 + \frac{m_{21}\tilde{\theta}}{\lambda_{y1}}\right)}. \quad (15)$$

Substituting the upper bound of (15) in (12), we attain a lower bound on P_{out1} as

$$P_{out1} > P_{out1}^{LB} = 1 - \frac{\left(\frac{m_1C_1}{\lambda_x} + \frac{m_1C_2\tilde{\theta}}{\lambda_x}\right)^{m_1}\left(\frac{m_{21}\tilde{\theta}}{\lambda_{y1}}\right)^{m_{21}}}{\Gamma(m_1)\Gamma(m_{21})} \times exp\left(-\frac{m_1C_1}{\lambda_x} - \frac{m_1C_2\tilde{\theta}}{\lambda_x}\right) \frac{1}{\left(1 + \frac{m_{21}\tilde{\theta}}{\lambda_{y1}}\right)} \times \sum_{n=0}^{\infty}\left(\frac{C_1}{C_1+C_2\tilde{\theta}}\right)^n \Psi\left(1+n, 1+m_{21}, \frac{m_{21}\tilde{\theta}}{\lambda_{y1}}\right) \times \Psi\left(1-n, 1+m_1-n, \frac{m_1C_1}{\lambda_x} + \frac{m_1C_2\tilde{\theta}}{\lambda_x}\right), \quad (16)$$

The rate outage probability of D2 is defined as the probability that the received SINR of D2 falls below the threshold, r_2 and is derived in Theorem 2. The upper and lower bounds on the rate outage probability of D2 are given as Corollary 2.1 and Corollary 2.2, respectively.

Theorem 2. *Let the random variables X, Y_1 and Y_2 be related to Z_2 and Z_3 through $Z_2 = \frac{aXY_2}{bXY_2+C_2Y_2+C_1}$ and $Z_3 = \frac{bXY_2}{C_2Y_2+C_1}$, then the rate outage at D_2 can be expressed as*

$$P_{out2} = 1 - \frac{\left(\frac{m_1C_1}{\lambda_x} + \frac{m_1C_2\tilde{\tau}}{\lambda_x}\right)^{m_1}\left(\frac{m_{22}\tilde{\tau}}{\lambda_{y2}}\right)^{m_{22}}}{\Gamma(m_1)\Gamma(m_{22})} \times exp\left(-\frac{m_1C_1}{\lambda_x} - \frac{m_1C_2\tilde{\tau}}{\lambda_x}\right) exp\left(-\frac{m_{22}\tilde{\tau}}{\lambda_{y2}}\right) \times \sum_{n=0}^{\infty}\left(\frac{C_1}{C_1+C_2\tilde{\tau}}\right)^n \Psi\left(1+n, 1+m_{22}, \frac{m_{22}\tilde{\tau}}{\lambda_{y2}}\right) \times \Psi\left(1-n, 1+m_1-n, \frac{m_1C_1}{\lambda_x} + \frac{m_1C_2\tilde{\tau}}{\lambda_x}\right). \quad (17)$$

Proof: Please refer to Appendix B.

Corollary 3. *Replace $\tilde{\theta}$ with $\tilde{\tau}$ in (13) and then substituting it's lower bound in (17), we get an upper bound on P_{out2} as*

$$P_{out2} \leq P_{out2}^{UB} = 1 - \frac{\left(\frac{m_1C_1}{\lambda_x}\right)^{m_1}\left(1 + \frac{m_1C_2\tilde{\tau}}{C_1}\right)\left(\frac{m_{22}\tilde{\tau}}{\lambda_{y2}}\right)^{m_{22}}}{\Gamma(m_1)\Gamma(m_{22})} \times exp\left(-\frac{m_1C_1}{\lambda_x} - \frac{m_1C_2\tilde{\tau}}{\lambda_x}\right) exp\left(-\frac{m_{22}\tilde{\tau}}{\lambda_{y2}}\right) \times \sum_{n=0}^{\infty}\left(\frac{C_1}{C_1+C_2\tilde{\tau}}\right)^n \Psi\left(1+n, 1+m_{22}, \frac{m_{22}\tilde{\tau}}{\lambda_{y2}}\right) \times \Psi\left(1-n, 1+m_1-n, \frac{m_1C_1}{\lambda_x} + \frac{m_1C_2\tilde{\tau}}{\lambda_x}\right). \quad (18)$$

Corollary 4. *Replace $\tilde{\theta}$ with $\tilde{\tau}$, λ_{y1} with λ_{y2} and m_{21} with m_{22} in (15). Then, substituting the upper bound of (15) in (17), we receive a lower bound on P_{out2} as*

$$P_{out2} > P_{out2}^{LB} = 1 - \frac{\left(\frac{m_1C_1}{\lambda_x} + \frac{m_1C_2\tilde{\tau}}{\lambda_x}\right)^{m_1}\left(\frac{m_{22}\tilde{\tau}}{\lambda_{y2}}\right)^{m_{22}}}{\Gamma(m_1)\Gamma(m_{22})} \times \Psi\left(1-n, 1+m_1-n, \frac{m_1C_1}{\lambda_x} + \frac{m_1C_2\tilde{\tau}}{\lambda_x}\right). \quad (19)$$

TABLE 3: Parameters and their values.

Parameter	Values	Parameter	Values
a_1	0.6	a_2	0.4
n_S	10^{-6}	n_R	10^{-6}
m_{RD_1}	{0.5-5}	m_{RD_2}	{0.5-5}
m_{SR}	{0.5-5}	ν	3
r_1	0.1 bps/Hz	r_2	0.1 bps/Hz
Ω_{RR}	-5dB	P_s/σ_R^2	15dB
D_{SR}	0.5		

B. SINR ANALYSIS

In this section, the average received SINR at D1, D1 relative to D2, and D2 are derived. Average SINR is a pivotal performance metric that can be used in multi-relay technologies to identify the ideal relay, as well as in other optimization techniques to attain a desirable limit.

Theorem 3. *Let* $Z_1 = \frac{aXY_1}{bXY_1+C_2Y_1+C_1}$ *represents the instantaneous SINR at destination* D_1*, then the average SINR* $\overline{Z}_1$ *can be written as*

$$\overline{Z}_1 = \left(\frac{a m_{21}}{b\Gamma(m_1)}\right)\left(\frac{C_1 m_{21}}{C_2\lambda_{y1}}\right)^{m_{21}} \sum_{n=0}^{\infty} \Gamma(1+m_1+n) \times \Psi\left(1+n, 1-m_1, \frac{m_1 C_2}{b\lambda_x}\right) \times \Psi\left(1+m_{21}, 1+m_{21}-n, \frac{C_1 m_{21}}{C_2\lambda_{y1}}\right). \quad (20)$$

Proof: Please refer to Appendix C.

Theorem 4. *Let the instantaneous SINR at* D_1 *relative to* D_2 *is* $Z_2 = \frac{aXY_2}{bXY_2+C_2Y_2+C_1}$*, then the average SINR* $\overline{Z}_2$ *can be expressed as*

$$\overline{Z}_2 = \left(\frac{a m_{22}}{b\Gamma(m_1)}\right)\left(\frac{C_1 m_{22}}{C_2\lambda_{y2}}\right)^{m_{22}} \sum_{n=0}^{\infty} \Gamma(1+m_1+n) \times \Psi\left(1+n, 1-m_1, \frac{m_1 C_2}{b\lambda_x}\right) \Psi\left(1+m_{22}, 1+m_{22}-n, \frac{C_1 m_{22}}{C_2\lambda_{y2}}\right). \quad (21)$$

Proof: Please refer to Appendix D.

Theorem 5. *Let* $Z_3 = \frac{bXY_2}{C_2Y_2+C_1}$ *denotes the instantaneous SINR at destination* D_2*, then the average SINR* $\overline{Z}_3$ *would become as*

$$\overline{Z}_3 = \left(\frac{b m_{22}\lambda_x}{C_2}\right)\Psi\left(1, 1-m_{22}, \frac{C_1 m_{22}}{C_2\lambda_{y2}}\right). \quad (22)$$

Proof: Please refer to Appendix E.

IV. RESULTS AND DISCUSSION

The derived analytical expressions are supported by numerical results for verification. For this, (24) is evaluated numerically for both cases. Without loss of generality, the analytical expressions' parameters are set as: a_1=0.6, a_2=0.4, σ_R^2=σ_D^2=1, ν=3 and $E\{|g_{ij}|^2\}$=1. Considering the linear topology, we have D_{SR}+D_{RD2}=0.75, D_{SR}+D_{RD1}=1 and chosen D_{SR}=0.5. The simulation results are obtained by considering more than 500,000 Monte Carlo runs. Tab. 3 shows the simulation parameters for the considered model [33].

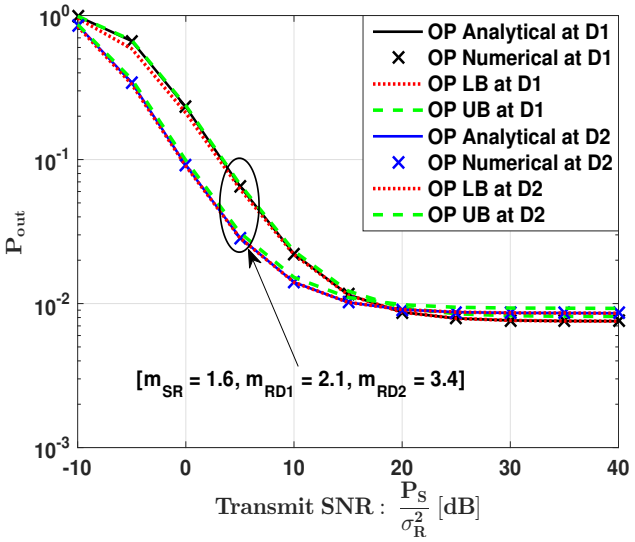

FIGURE 2: Rate outage analysis of the proposed system. $(r_1 = r_2, \Omega_{RR}) = (0.5, -5dB)$

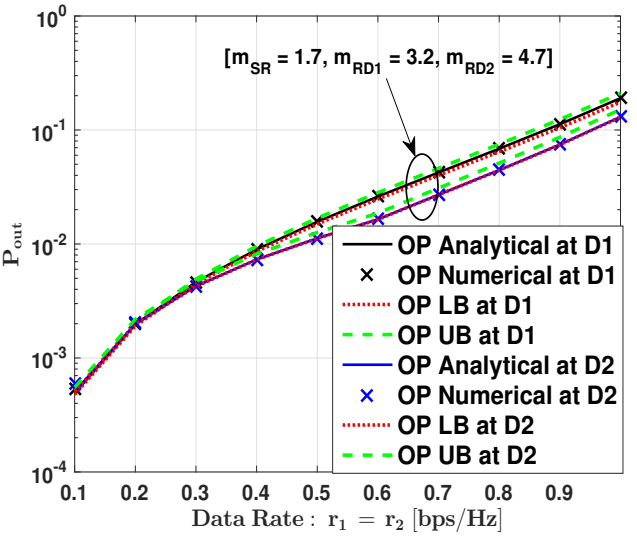

FIGURE 3: Rate outage analysis of the proposed system. $\left(\Omega_{RR}, \frac{P_S}{\sigma_R^2}\right) = (-5dB, 10dB)$.

Rate outage analysis of the considered system versus various parameters is presented in this section. Fig. 2 shows the rate outage performance of the two users at D_1 and D_2 against the transmit SNR. It can be noted that the performance of user at D_2 is superior than the user at D_1 at low SNR values. This may be attributed to the fact that former is a strong user compared to the later. However, the rate outage performance of both users saturates when $\frac{P_S}{\sigma_R^2} \geq 15dB$ as shown in this

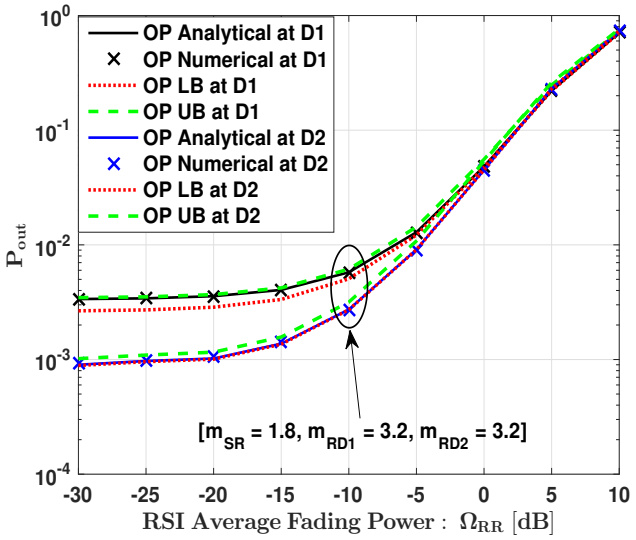

FIGURE 4: Rate outage analysis of the proposed system. $\left(\frac{P_S}{\sigma_R^2}, r_1 = r_2\right) = (10dB, 0.5)$.

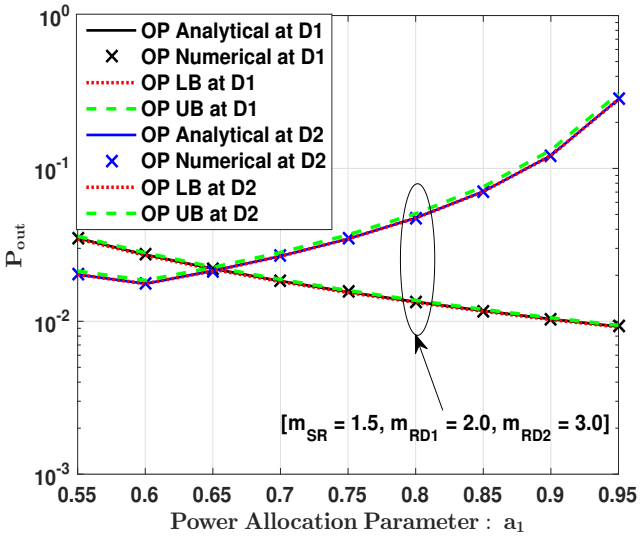

FIGURE 5: Rate outage analysis of the proposed system. $\left(\frac{P_S}{\sigma_R^2}, r_1 = r_2, \Omega_{RR}\right) = (10dB, 0.5, -5dB)$.

figure. This may be associated to the deteriorating impact of RSI due to full-duplex relaying on the system's performance in this SNR range. Moreover, it can be observed from this figure that the upper and lower bounds on outage probabilities are tight in the whole SNR regime.

Outage behaviour versus the target data rate is depicted in Fig. 3. Chances of outage occurrence increase by increasing the target data rate as observed in this figure. Moreover, it is again evident that the user at D_2 has better outage performance than the user at D_1 at higher target data rates. However, the performance gap between the two users becomes insignificant at small data rate values. This fact describes that strong and weak users have similar performance in this range. Moreover, the upper and lower bounds are tightly close to the exact outage probabilities as shown in the figure.

Fig. 4 highlights the impact of average RSI fading channel's power on the outage performance. The outage performance of the user at D_2 is streets ahead than the user at D_1 at very small RSI fading channel power values. However, the performance of the two users severely degrades when RSI power $> -5dB$ as observed in this figure. This fact again reflects that there is no performance difference between the strong and weak users at large power values of the RSI fading channel. Similarly, the upper and lower bounds maintain consistent gap with exact outage probabilities.

Outage variations versus power allocation parameter a_1 are depicted in Fig. 5. It can be noted from this figure that the performance of user at D_2 is better than the user at D_1 when $a_1 < 0.65$. However, the outage performance of user at D_1 improves rapidly when more power is allocated to symbol 1. Furthermore, the upper and lower bounds are consistently tight in whole range of values of the parameter a_1. It is pertinent to mention here that analytical results perfectly match the numerical results verifying their accuracy.

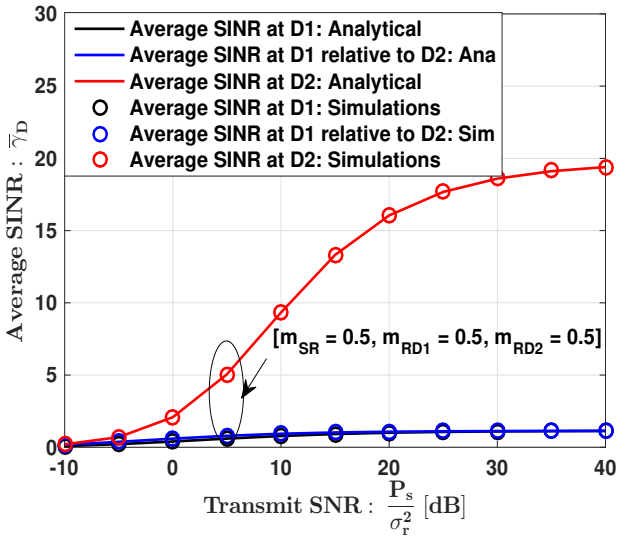

FIGURE 6: Average SINR analysis of the proposed system. $(D_{SR}, \Omega_{RR}) = (0.4, -5dB)$

The results for average SINR analysis are presented against different parameters. For simulation purposes, 5×10^6 independent samples of Nakagami-m distributed random variables are generated to corroborate the analytical expressions. The rest of the parameter values in the evaluation of analytical expressions are same except D_{SR}=0.4.

Fig. 6 shows the average received SINR versus the transmit SNR when the $S-R$, $R-D_1$ and $R-D_2$ links suffers from worst than Rayleigh fading. It can be observed from this figure that average received SINR increases with increase in transmit SNR as expected. However, it is sufficiently low at

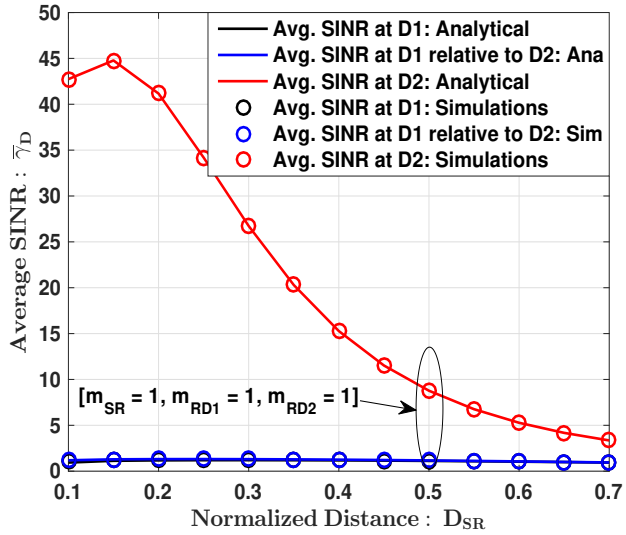

FIGURE 7: Average SINR analysis of the proposed system. $\left(\Omega_{RR}, \frac{P_S}{\sigma_R^2}\right) = (-5dB, 15dB)$.

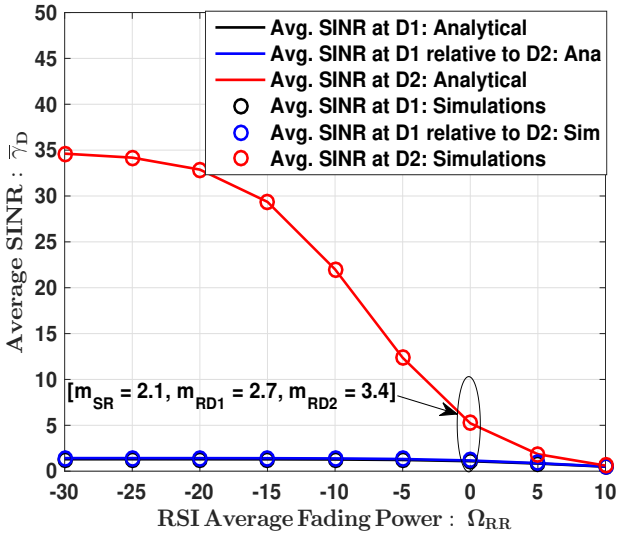

FIGURE 8: Average SINR analysis of the proposed system. $\left(\frac{P_S}{\sigma_R^2}, D_{SR}\right) = (10dB, 0.4)$

destination D_1 compared to destination D_2. This behavior is due to the fact that symbol $s_2(t)$ is present as interference in the instantaneous SINR received at destination D_1 whereas the interference of symbol $s_1(t)$ is removed from the instantaneous SINR received at destination D_2. At D_2, the average received SINR saturates at high SNR values because of the RSI due to full-duplex relaying. Moreover, the performance gap between the two average received SINR graphs at destination D_1 is insignificant.

Average received SINR graphs against the normalized $S-R$ distance are shown in Fig. 7. The fading at the three links is assumed to be Rayleigh distributed. It can be noticed from this figure that the average received SINR at destination D_2 is significantly high when the relay is close to the source node. This behavior may be attributed to the fact that the gain provided by the relay depends on $S-R$ channel average statistics. However, there is no remarkable impact of relay location on the average received SINR at destination D_1 due to the presence of symbol $s_2(t)$ as interference.

The influence of average RSI fading power on average received SINR is exhibited in Fig. 8. The $R-D_1$ and $R-D_2$ links are less faded as compared to $S-R$ link in order to study their impact on the average received SINR in the considered scenario. It is evident from this figure that average received SINR at destination D_2 decreases rapidly with increase in average power of RSI. However, this impact is invisible in the average received SINR at destination D_1.

Fig. 9 elaborates average received SINR against power allocation parameter a_1. The $S-R$ link is considered less faded compared to $R-D_1$ and $R-D_2$ links to highlight it's impact on average received SINR. It can be seen that the average received SINR at destination D_2 decreases rapidly whereas at destination D_1, it gradually improves by increasing the

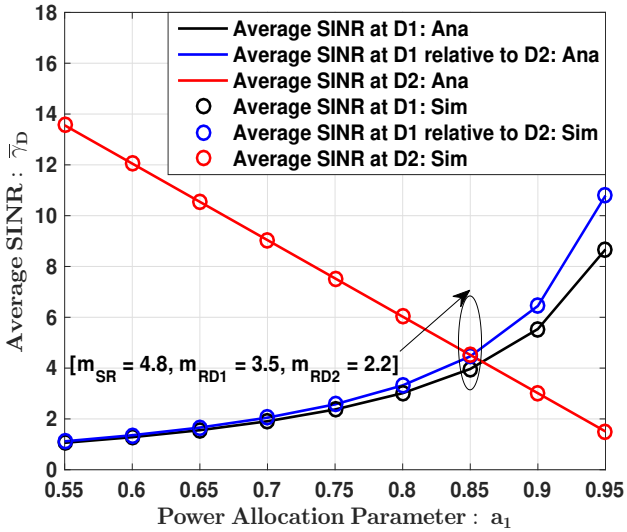

FIGURE 9: Average SINR analysis of the proposed system. $\left(\frac{P_S}{\sigma_R^2}, \Omega_{RR}\right) = (10dB, -5dB)$.

values of a_1 as shown in the figure. It is advantageous to mention here that simulations perfectly support the analytical expressions.

Convergence of series' in outage expressions (12 - 19) is shown in Fig. 10. It is evident from this figure that first few terms are sufficient for the convergence of series' in the given expressions verifying their efficient evaluation.

Convergence of series' in average SINR expressions (20 - 21) is displayed in Fig. 11. It is clear from this figure that series' converge quickly with few number of terms. These graphs certify the good convergence efficiency of our

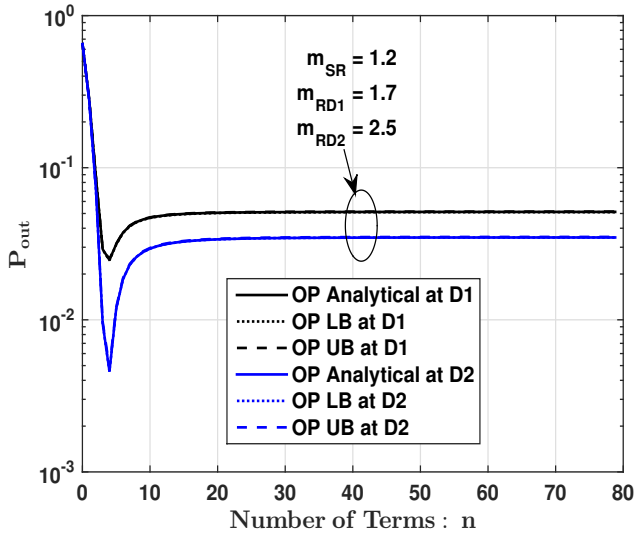

FIGURE 10: Convergence of Series' with considered parameters: $\left(\frac{P_S}{\sigma_R^2}, r_1 = r_2, , \Omega_{RR}\right) = (10dB, 0.5, -5dB)$.

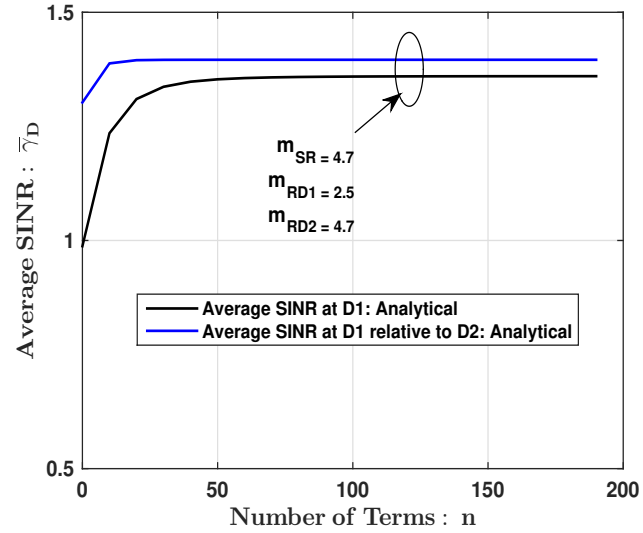

FIGURE 11: Convergence of Series' with considered parameters: $\left(\frac{P_S}{\sigma_R^2}, \Omega_{RR}\right) = (15dB, -5dB)$.

proposed analytical expressions.

V. CONCLUSIONS

The rate outage and average SINR of a NOMA-coordinated dual-hop FD-AF vehicle-to-vehicle relaying over Nakagami-m fading channels are analyzed considering the repercussions of RSI due to full-duplex relaying. Closed-form expressions of rate outage probabilities and average received SINRs are acquired for two vehicular users at different destinations. The derived analytical expressions work for any values of the fading parameter m. Moreover, the lower and upper bounds are deduced from the obtained outage expressions. Analytical and simulation results perfectly coincides verifying the correctness of the proposed results. The application significance of this study lies in improving the accuracy as well as effectiveness of V2V connectivity in autonomous vehicles. The paper provides illumination on boosting FD-AF relaying for automobiles systems by examining rate disruption and average SINR. The obtained closed-form equations aid in the development of resilient methods for communication capable of maintaining consistent connection throughout fading and disruption. This research is especially important for developing applications that require safety, self-driving cars and cost-effective data transmission in vehicle networks.

APPENDIX A PROOF OF THEOREM 1

The rate outage can be defined as P_{out1}=$F_{Z_1}(\theta)|_{\theta=2^{r_1}-1}$ [33], where r_1 is the target rate in bits per second per Hertz (bps/Hz) at D_1. Then the probability of rate outage at D_1 can be written as

$$\begin{aligned} P_{out1} &= P\left(\frac{aXY_1}{bXY_1 + C_2Y_1 + C_1} < \theta\right) \\ &= P\left(X < C_2\tilde{\theta}\frac{\left(Y_1 + \frac{C_1}{C_2}\right)}{Y_1}\right) \\ &= F_X\left(C_2\tilde{\theta}\frac{\left(Y_1 + \frac{C_1}{C_2}\right)}{Y_1}\right), \end{aligned} \tag{23}$$

where $\tilde{\theta}$=$\frac{\theta}{a-b\theta}$ subject to the condition that $\frac{a}{b} > \theta$. Invoking the law of total probability and using (8), we get

$$\begin{aligned} P_{out1} &= \int_0^{\tilde{\theta}} f_{Y_1}(y_1)\, dy_1 \\ &\quad + \int_{\tilde{\theta}}^{\infty}\left(1 - \frac{1}{\Gamma(m_1)}\Gamma\left(m_1, \frac{m_1C_2\tilde{\theta}}{\lambda_x}\frac{\left(y_1 + \frac{C_1}{C_2}\right)}{y_1}\right)\right) f_{Y_1}(y_1)\, dy_1, \\ &= 1 - \frac{1}{\Gamma(m_1)}\int_{\tilde{\theta}}^{\infty}\Gamma\left(m_1, \frac{m_1C_2\tilde{\theta}}{\lambda_x}\frac{\left(y_1 + \frac{C_1}{C_2}\right)}{y_1}\right) f_{Y_1}(y_1)\, dy_1, \end{aligned} \tag{24}$$

where we have leveraged from the identity $\int_0^{\tilde{\theta}} f_{Y_1}(y_1)\, dy_1$ + $\int_{\tilde{\theta}}^{\infty} f_{Y_1}(y_1)\, dy_1$=1. The expression (24) can further be simplified by substituting $y_1 - \tilde{\theta}$=u, then P_{out1} will become

$$P_{out1} = 1 - \frac{1}{\Gamma(m_1)}\int_0^{\infty}\Gamma\left(m_1, \frac{m_1C_2\tilde{\theta}}{\lambda_x}\frac{u + \tilde{\theta} + \frac{C_1}{C_2}}{u + \tilde{\theta}}\right) f_{Y_1}\left(u + \tilde{\theta}\right) du. \tag{25}$$

Now using (7) and writing $\Gamma(\cdot,\cdot)$ in terms of Fox's H-function [41], we obtain

$$P_{out1} = 1 - \frac{\left(\frac{m_{21}}{\lambda_{y1}}\right)}{\Gamma(m_1)\Gamma(m_{21})} \int_0^\infty \times H_{1,2}^{2,0}\left[\frac{m_1 C_2 \tilde{\theta}}{\lambda_x} \times \frac{u+\tilde{\theta}+\frac{C_1}{C_2}}{u+\tilde{\theta}} \middle| \begin{matrix}(1,1)(m_1,1),(0,1)\end{matrix}\right] \times H_{0,1}^{1,0}\left[\frac{m_{21}}{\lambda_{y1}}(u+\tilde{\theta}) \middle| \begin{matrix}(m_{21}-1,1)\end{matrix}\right] du. \quad (26)$$

A convenient way to solve (26) is by using the definition of Fox's H-function [38, Eq. (1.1.1)] which will lead to

$$P_{out1} = 1 - \frac{\left(\frac{m_{21}}{\lambda_{y1}}\right)}{\Gamma(m_1)\Gamma(m_{21})} \frac{1}{(2\pi\imath)^2} \int_{\mathfrak{L}_1}\int_{\mathfrak{L}_2} \frac{\Gamma(m_1-s)\Gamma(-s)}{\Gamma(1-s)} \times \Gamma(m_{21}-1-t)\left(\frac{m_1 C_2 \tilde{\theta}}{\lambda_x}\right)^s \left(\frac{m_{21}}{\lambda_{y1}}\right)^t \times \underbrace{\int_0^\infty \left(u+\tilde{\theta}+\frac{C_1}{C_2}\right)^s (u+\tilde{\theta})^{t-s} du}_{I_1} ds\, dt. \quad (27)$$

The integral I_1 can be evaluated using [37, Eq. (3.197.1)] as

$$I_1 = (\tilde{\theta})^{1+t}\left(\frac{C_1+C_2\tilde{\theta}}{C_2\tilde{\theta}}\right)^s B(1,-1-t) \times {}_2F_1\left(-s,1;-t;\frac{C_1}{C_1+C_2\tilde{\theta}}\right), \; Re\{t\} < -1 \quad (28)$$

where $B(\cdot,\cdot)$ is the beta function [37, Eq. (8.380.1)] and ${}_2F_1(\cdot,\cdot;\cdot;\cdot)$ is the hypergeometric function [37, Eq. (9.111)]. Now I_1 can be simplified by making use of the identities [37, Eq. (8.384.1)], [37, Eq. (9.100)], [37, Eq. (8.338.1)] and [37, Eq. (8.339.1)] resulting in

$$I_1 = (\tilde{\theta})^{1+t}\left(\frac{C_1+C_2\tilde{\theta}}{C_2\tilde{\theta}}\right)^s \frac{\Gamma(-1-t)}{\Gamma(-s)} \times \sum_{n=0}^\infty \frac{\Gamma(n-s)}{\Gamma(n-t)}\left(\frac{C_1}{C_1+C_2\tilde{\theta}}\right)^n. \quad (29)$$

Substituting I_1 in (27), we get

$$P_{out1} = 1 - \frac{\left(\frac{m_{21}\tilde{\theta}}{\lambda_{y1}}\right)}{\Gamma(m_1)\Gamma(m_{21})} \sum_{n=0}^\infty \left(\frac{C_1}{C_1+C_2\tilde{\theta}}\right)^n \times \frac{1}{(2\pi\imath)}\int_{\mathfrak{L}_1} \frac{\Gamma(m_1-s)\Gamma(n-s)}{\Gamma(1-s)}\left(\frac{m_1C_1}{\lambda_x}+\frac{m_1C_2\tilde{\theta}}{\lambda_x}\right)^s ds \times \frac{1}{(2\pi\imath)}\int_{\mathfrak{L}_2} \frac{\Gamma(m_{21}-1-t)\Gamma(-1-t)}{\Gamma(n-t)}\left(\frac{m_{21}\tilde{\theta}}{\lambda_{y1}}\right)^t dt. \quad (30)$$

Exploiting [38, Eq. (1.1.1)] and [38, Eq. (1.7.1)], we obtain

$$P_{out1} = 1 - \frac{\left(\frac{m_{21}\tilde{\theta}}{\lambda_{y1}}\right)}{\Gamma(m_1)\Gamma(m_{21})} \sum_{n=0}^\infty \left(\frac{C_1}{C_1+C_2\tilde{\theta}}\right)^n \times G_{1,2}^{2,0}\left(\frac{m_1C_1}{\lambda_x}+\frac{m_1C_2\tilde{\theta}}{\lambda_x}\middle| \begin{matrix}1\\ m_1,n\end{matrix}\right) \times G_{1,2}^{2,0}\left(\frac{m_{21}\tilde{\theta}}{\lambda_{y1}}\middle| \begin{matrix}n\\ m_{21}-1,-1\end{matrix}\right), \quad (31)$$

where $G_{p,q}^{m,n}(\cdot)$ is the Meijer's G-function [38, Eq. (1.7.1)]. The expression (31) reduces to (12) by making use of [42] which completes the proof. ■

APPENDIX B PROOF OF THEOREM 2

The probability of rate outage P_{out2} with $\theta = 2^{r_2}-1$, where r_2 is the target rate in bps/Hz at D_2, can be expressed as

$$P_{out2} = P\left(\frac{aXY_2}{bXY_2+C_2Y_2+C_1} < \theta\right) + P\left(\frac{bXY_2}{C_2Y_2+C_1} < \theta, \frac{aXY}{bXY+C_2Y+C_1} > \theta\right). \quad (32)$$

The expressions in (32) can be simplified as

$$P\left(\frac{aXY_2}{bXY_2+C_2Y_2+C_1} < \theta\right) = P\left((a-b\theta)XY_2 < \theta(Y_2C_2+C_1)\right) = P\left(\frac{XY_2}{C_2Y_2+C_1} < \frac{\theta}{a-b\theta} \triangleq \tilde{\theta}\right). \quad (33)$$

Thus, the probability expression can be written as

$$P\left(\frac{bXY_2}{C_2Y_2+C_1} < \theta\right) = P\left(\frac{XY_2}{C_2Y_2+C_1} < \frac{\theta}{b} \triangleq \acute{\theta}\right). \quad (34)$$

Substituting (33) and (34) in (32) and using the statistical identity $P(C,D)$=$P(C)$-$P\left(C,\overline{D}\right)$, P_{out2} becomes

$$P_{out2} = P\left(\frac{XY_2}{C_2Y_2+C_1} < \tilde{\theta}\right) + P\left(\frac{XY_2}{C_2Y_2+C_1} < \acute{\theta}\right) - P\left(\frac{XY_2}{C_2Y_2+C_1} < \tilde{\theta}, \frac{XY_2}{C_2Y_2+C_1} < \acute{\theta}\right). \quad (35)$$

Now P_{out2} can be re-written as

$$P_{out2} = P\left(\frac{XY_2}{C_2Y_2+C_1} < max\left\{\tilde{\theta},\acute{\theta}\right\} \triangleq \tilde{\tau}\right) = F_X\left(C_2\tilde{\tau}\frac{\left(Y_2+\frac{C_1}{C_2}\right)}{Y_2}\right). \quad (36)$$

The rest of the procedure is same as derived in *Theorem 1* and the proof is completed. ■

APPENDIX C PROOF OF THEOREM 3

The instantaneous SINR at destination D_1 can be re-written as

$$Z_1 = \frac{\left(\frac{a}{b}\right)X}{X+A}, \quad (37)$$

where $A=\frac{C_2Y_1+C_1}{bY_1}$. The average SINR can then be computed as

$$\overline{Z}_1 = \frac{\left(\frac{a}{b}\right)\left(\frac{m_{21}}{\lambda_{y1}}\right)^{m_{21}}}{\Gamma(m_{21})}\int_0^{\infty}\underbrace{\frac{\left(\frac{m_1}{\lambda_x}\right)^{m_1}}{\Gamma(m_1)}\int_0^{\infty}\frac{x^{m_1}}{x+A}exp\left(-\frac{m_1}{\lambda_x}x\right)dx}_{I2} \times f_{Y_1}(y_1)\,dy_1. \quad (38)$$

The integral I_2 can be evaluated using [37, Eq. (3.383.10)]. Then it can be simplified using [37, Eq. (8.331.1)] and [37, Eq. (8.351.4)] resulting in the form as

$$I_2 = m_1\Psi\left(1, 1-m_1, \frac{m_1C_2}{b\lambda_x}+\frac{m_1C_1}{b\lambda_x y_1}\right). \quad (39)$$

The result of I_2 can further be expanded using the identity [43, Eq. (13.13.9)] as

$$I_2 = \frac{y_1}{\Gamma(m_1)}\sum_{n=0}^{\infty}\Gamma(1+m_1+n)\frac{\left(\frac{C_1}{C_2}\right)^n}{\left(\frac{C_1}{C_2}+y_1\right)^{n+1}} \Psi\left(1+n, 1-m_1, \frac{m_1C_2}{b\lambda_x}\right). \quad (40)$$

Substituting the value of I_2 in (38), we obtain

$$\overline{Z}_1 = \frac{\left(\frac{a}{b}\right)\left(\frac{m_{21}}{\lambda_{y1}}\right)^{m_{21}}}{\Gamma(m_1)\Gamma(m_{21})}\sum_{n=0}^{\infty}\Gamma(1+m_1+n)\left(\frac{C_1}{C_2}\right)^n \Psi\left(1+n, 1-m_1, \frac{m_1C_2}{b\lambda_x}\right) \times \underbrace{\int_0^{\infty}\frac{y_1^{m_{21}}}{\left(\frac{C_1}{C_2}+y_1\right)^{n+1}}exp\left(-\frac{m_{21}}{\lambda_{y1}}y_1\right)dy_1}_{I_3}. \quad (41)$$

The integral I_3 can evaluated using [44, Eq. (2.3.6.9)] giving

$$I_3 = \Gamma(1+m_{21})\left(\frac{C_1}{C_2}\right)^{m_{21}-n}\Psi\left(1+m_{21}, 1+m_{21}-n, \frac{C_1m_{21}}{C_2\lambda_{y_1}}\right). \quad (42)$$

Substituting the value of I_3 in (41) results in (20) which completes the proof. ■

APPENDIX D PROOF OF THEOREM 4

The procedure for the proof of *Theorem 4* is same as that of *Theorem 3*. ■

APPENDIX E PROOF OF THEOREM 5

The instantaneous SINR at destination D_2 can be re-written as

$$Z_3 = \frac{b}{C_2}\frac{XY_2}{Y_2+\frac{C_1}{C_2}}. \quad (43)$$

The average SINR can be calculated as

$$\overline{Z}_3 = \underbrace{\frac{\left(\frac{b}{C_2}\right)\left(\frac{m_1}{\lambda_x}\right)^{m_1}}{\Gamma(m_1)}\int_0^{\infty}x^{m_1}exp\left(-\frac{m_1}{\lambda_x}x\right)dx}_{I_4} \times \underbrace{\frac{\left(\frac{m_{22}}{\lambda_{y2}}\right)^{m_{22}}}{\Gamma(m_{22})}\int_0^{\infty}\frac{y_2^{m_{22}}}{\left(\frac{C_1}{C_2}+y_2\right)}exp\left(-\frac{m_{22}}{\lambda_{y_2}}y_2\right)dy_2}_{I_5}. \quad (44)$$

Now I_4 can be solved [37, Eq. (3.326.2)] and simplified [37, Eq. (8.331.1)] producing the output as

$$I_4 = \frac{b}{C_2}\lambda_x. \quad (45)$$

Similarly, I_5 can be solved [37, Eq. (3.383.10)] and further simplified making use of [37, Eq. (8.331.1)] and [37, Eq. (8.351.4)] as

$$I_5 = m_{22}\Psi\left(1, 1-m_{22}, \frac{C_1m_{22}}{C_2\lambda_{y2}}\right). \quad (46)$$

Substituting (45) and (46) in (44) completes the proof. ■

REFERENCES

[1] A. Tregancini, E. E. B. Olivo, D. P. M. Osorio, C. H. M. de Lima, and H. Alves, "Performance analysis of Full-Duplex relay-aided NOMA systems using partial relay selection," ITVT, vol. 69, pp. 622–635, Jan. 2020.

[2] N. Jaiswal, A. Pandey, S. Yadav, N. Purohit, and D. S. Gurjar, "Physical layer security performance of NOMA-aided vehicular communications over nakagami-*m* time-selective fading channels with channel estimation errors," IEEE Open Journal of Vehicular Technology, vol. 4, pp. 72–100, 2022.

[3] H. U. Khan, F. Ali, M. Sohail, S. Nazir, and M. Arif, "Decision making for selection of smart vehicle transportation system using VIKOR approach," International Journal of Data Science and Analytics, pp. 1–15, 2024.

[4] A.-B. Yakubu, A. H. Abd El-Malek, M. Abo-Zahhad, O. Muta, and M. M. Elsabrouty, "Task offloading and resource allocation in an RIS-assisted NOMA-based vehicular edge computing," IEEE Access, 2024.

[5] M. Arif and W. Kim, "Analysis of U-V2X communications with non-clustered and clustered jamming in the presence of fluctuating UAV beam width," Mathematics, vol. 11, no. 15, p. 3434, 2023.

[6] M. Arif and W. Kim, "Clustered jamming in U-V2X communications with 3D antenna beam-width fluctuations," Computer Communications, vol. 216, pp. 209–228, 2024.

[7] Y. M. Khattabi, S. A. Alkhawaldeh, M. M. Matalgah, O. S. Badarneh, and R. Mesleh, "Vehicle-to-roadside-unit-to-vehicle communication system under different amplify-and-forward relaying schemes," Vehicular Communications, vol. 38, p. 100539, 2022.

[8] C. Li, W. Chen, Z. Pei, F. Chang, J. Yu, and F. Luo, "Non-stationary time-varying vehicular channel characteristics for different roadside scattering environments," Scientific Reports, vol. 12, no. 1, p. 14344, 2022.

[9] M. Noor-A-Rahim, Z. Liu, H. Lee, M. O. Khyam, J. He, D. Pesch, K. Moessner, W. Saad, and H. V. Poor, "6g for vehicle-to-everything (V2X) communications: Enabling technologies, challenges, and opportunities," Proceedings of the IEEE, vol. 110, no. 6, pp. 712–734, 2022.

[10] N. Shende, O. Gurbuz, and E. Erkip, "Half-duplex or full-duplex relaying: A capacity analysis under self-interference," in 2013 47th Annual Conference on Information Sciences and Systems (CISS), pp. 1–6, IEEE, 2013.

[11] T. T. Nguyen, M. H. Tran, T. T. H. Le, X. N. Tran, et al., "Joint resource and trajectory optimization for secure UAV-based relay NOMA system," Vehicular Communications, vol. 43, p. 100650, 2023.

[12] S. Singh and M. Bansal, "On the performance of STBC-NOMA assisted overlay cognitive system under CEEs and imperfect SIC," Vehicular Communications, vol. 39, p. 100546, 2023.

[13] H. H. Jeong, Y. C. Shen, J. P. Jeong, and T. T. Oh, "A comprehensive survey on vehicular networking for safe and efficient driving in smart transportation: A focus on systems, protocols, and applications," Vehicular Communications, vol. 31, p. 100349, 2021.
[14] C. Guo, L. Zhao, C. Feng, Z. Ding, and H.-H. Chen, "Energy harvesting enabled NOMA systems with Full-Duplex relaying," ITVT, vol. 68, pp. 7179–7183, Jul. 2019.
[15] R. Ma, L. Wang, M. Pan, and L. Xu, "Enabling edge caching through Full-Duplex Non-Orthogonal Multiple Access," ITVT, vol. 69, pp. 12338–12342, Oct. 2020.
[16] O. Abbasi and H. Yanikomeroglu, "Transmission scheme, detection and power allocation for uplink user cooperation with NOMA and RSMA," ITWC, vol. 22, pp. 471–485, Jan. 2023.
[17] O. S. Badarneh, M. K. Awad, S. Muhaidat, and F. S. Almehmadi, "Performance analysis of intelligent reflecting surface-aided decode-and-forward UAV communication systems," IEEE Systems Journal, vol. 17, no. 1, pp. 246–257, 2022.
[18] G. Levin and S. Loyka, "Amplify-and-forward versus decode-and-forward relaying: Which is better?," in 22th International Zurich seminar on communications (IZS), Eidgenössische Technische Hochschule Zürich, 2012.
[19] A. Mukherjee, P. Chakraborty, S. Prakriya, and A. K. Mal, "Cooperative mode switching-based cognitive NOMA with transmit antenna and user selection," ITSIPN, vol. 8, pp. 932–945, Nov. 2022.
[20] C. Campolo, A. Molinaro, A. O. Berthet, and A. Vinel, "Full-duplex radios for vehicular communications," IEEE Communications Magazine, vol. 55, no. 6, pp. 182–189, 2017.
[21] Y. Ai, M. Cheffena, A. Mathur, and H. Lei, "On physical layer security of double rayleigh fading channels for vehicular communications," IEEE Wireless Communications Letters, vol. 7, no. 6, pp. 1038–1041, 2018.
[22] S. Shailendra and B. Matadeen, "Performance analysis of uplink NOMA-assisted Full-Duplex Amplify-and-Forward CR network," in IISPC, pp. 1–5, 2022.
[23] J. Jose, P. Shaik, and V. Bhatia, "VFD-NOMA under imperfect SIC and residual inter-relay interference over generalized Nakagami-*m* fading channels," ICL, vol. 27, pp. 507–511, Feb. 2021.
[24] T. Bhavsar and A. Jindal, "On reducing the outage probability in VFD-NOMA with limited CSI at source," ICL, vol. 25, pp. 646–650, Oct. 2023.
[25] S. H. Alvi, "Moments and outage analysis of NOMA-based AF relaying system over Nakagami-*m* fading channels," IJEC, vol. 162, pp. 1–8, Feb. 2023.
[26] X. Yue, Y. Liu, S. Kang, and A. Nallanathan, "Performance analysis of NOMA with fixed gain relaying over Nakagami-*m* fading channels," IEEE Access, vol. 5, pp. 5445–5454, May 2017.
[27] Ashish and P. Kumar, "NOMA communication system assisted with IRS and relay transmission," SP, vol. 220, p. 109441, 2024.
[28] D. Wan, M. Wen, F. Ji, Y. Liu, and Y. Huang, "Cooperative NOMA systems with partial channel state information over Nakagami-*m* fading channels," ITC, vol. 66, pp. 947–958, Mar. 2018.
[29] S. Li, X. Dang, X. Yu, C. Hao, J. Li, and M. Feng, "Transceiver design for an uplink asynchronous NOMA using MSK-type signals," SP, vol. 212, p. 109166, 2023.
[30] A. F. Molisch, Wireless Communications. Chichester, UK: Wiley-IEEE Press, second ed., 2011.
[31] M. K. Simon and M.-S. Alouini, Digital Communications over Fading Channels. New York: Wiley, second ed., 2005.
[32] M. Uysal, Cooperative Communications for improved wireless network transmission: Framework for virtual antenna array applications. Hershey, New York: Information Science Reference, 2009.
[33] O. Abbasi, A. Ebrahimi, and N. Mokari, "NOMA inspired cooperative relaying system using an AF relay," IWCL, vol. 8, pp. 261–264, Feb. 2019.
[34] A. Gupta, M. Sellathurai, and T. Ratnarajah, "End-to-End learning-based Full-Duplex Amplify-and-Forward relay networks," ITC, vol. 71, pp. 199–213, Jan. 2023.
[35] B. C. Nguyen, X. N. Tran, D. T. Tran, and L. T. Dung, "Full-duplex Amplify-and-Forward relay system with direct link: Performance analysis and optimization," PC, vol. 37, pp. 1–10, Oct. 2019.
[36] M. Dohler and Y. Li, Cooperative Communications: Hardware, Channel and PHY. West Sussex, UK: John Wiley and Sons, 2010.
[37] I. S. Gradshteyn and I. M. Ryzhik, Table of Integrals, Series and Products. Burlington, MA: Academic Press, seventh ed., 2007.
[38] A. M. Mathai and R. K. Saxena, The H-Function with applications in statistics and other disciplines. New York, USA: John Wiley & Sons, 1978.
[39] B. Laxmi and A. V. Laxmi, "Subadditive and completely monotonic properties of the tricomi confluent hypergeometric functions," Int. Jour. Adv. in Math., vol. 2018, no. 5, pp. 25–33, 2018.
[40] M. Abramowitz and I. A. Stegun, Handbook of Mathematical Functions with Formulas, Graphs and Mathematical Tables. New York: Dover, tenth ed., 1972.
[41] C. D. Bodenschatz, Finding an H-function distribution for the sum of independent H-function variates. PhD thesis, The University of Texas at Austin, USA, 1992.
[42] E. W. Weisstein, "Meijer's G-function [online]. available at:." https://functions.wolfram.com/HypergeometricFunctions/MeijerG/03/01/04/12/0002/, 2023. Accessed: 2023-09-30.
[43] F. W. Olver, D. W. Lozier, R. S. Boisvert, and C. W. Clark, NIST Handbook of Mathematical Functions. New York: Cambridge University Press, 2010.
[44] A. P. Prudnikov, Y. A. Brychkov, and O. I. Marichev, Integrals and Series: Elementary Functions. USSR Academy of Sciences, Moscow: Gordon and Breach Science Publishers, 1986.

SAJID HUSSAIN ALVI received his MSc and MPhil degrees in Electronics from Quaid-e-Azam University Islamabad, Pakistan in 2001 and 2006, respectively. He received his PhD from department of Electrical Engineering, COMSATS Institute of Information Technology (CIIT), presently COMSATS University Islamabad (CUI), Islamabad, Pakistan in 2017. Since 2006 he is serving as a faculty member at CUI where he is currently an assistant professor at the Department of Physics. Dr. Alvi's research interests are in cooperative communications, terrestrial and aerial heterogeneous networks, Terahertz (THz) communications and Metamaterials.

MOHAMMAD ARIF received a B.S. degree in electrical engineering from the University of Engineering and Technology, Peshawar, Pakistan, in 2012 and the M.S. and Ph.D. degrees in electrical engineering from the COMSATS University Islamabad, Pakistan, in 2014 and 2021, respectively. Currently, he is working as an Assistant Professor in the Department of Computer Engineering at Gachon University, Seongnam, South Korea. He has also served as a visiting research associate at Qatar University, Doha, Qatar, in 2022. His research interests include U-V2X communications, jamming interference, mm-Waves communications, C-V2X communications, aerial and terrestrial heterogeneous networks, dual connectivity, decoupled access, interference management, reverse frequency allocation, indoor localization, signal processing, and channel coding.

KEIVAN NAVAIE (Senior Member, IEEE) is a Principal and AI Technology Advisor at the Information Commissioner Office (U.K. Data Protection Regulatory Body), and a Chair Professor in Intelligent Networks at the School of Computing and Communications, Lancaster University. He has an interdisciplinary research portfolio seeking innovative solutions to address fundamental technical and design challenges in intelligent cyber-physical systems and their applications in reducing carbon-foot print in day-to-day life activities. His research topics include deep learning, privacy enhanced AI, AI regulations, distributed and federated AI, connectivity resilience incyber-physical systems and the IoT, machine learning and artificial intelligence applications, cognitive communications networks, and cryptosystems. He has actively contributed to evidence-based policymaking through involvement with the United Nations' International Telecommunications Union (ITU), EU Environment Agency, Information Commissioner's Office, and EU Parliament. He is a Fellow of IET, a Chartered Engineer in the U.K., and a Senior Fellow of the HEA. He is on the editorial board of the IEEE TRANSACTIONS ON WIRELESS COMMUNICATIONS, the IEEE COMMUNICATIONS SURVEYS AND TUTORIAL, and the IEEE Communication Letters.